Garcia Bernabe, A.; Rivera-Sancho, A.; Granados; Adrián; Luis, SV.; Compañ Moreno, V. (2016). Ionic transport on composite polymers containing covalently attached and absorbed ionic liquid fragments. Electrochimica Acta. 213:887-897. doi:10.1016/j.electacta.2016.08.018.

Ionic transport on composite polymers containing covalently attached and absorbed ionic liquid fragments

Abel García-Bernabé[1], Angel Rivera[1], Adrián Granados[2], Santiago V. Luis[2], Vicente Compañ[1,*]

[1] Dpto. Termodinámica Aplicada. Universidad Politécnica de Valencia. Camino de Vera s/n 46022-Valencia (Spain)

[2] Dpto. Química Inorgánica y orgánica. Universidad Jaume I, Avda. Sos, Baynat s/n 12071 Castellón (Spain)

Abstract: *The ionic transport of five supported ionic liquid-like phases (SILLPs) based on 1-butyl imidazolium ion covalently attached to a polymeric matrix has been analysed by means of electrochemical impedance spectroscopy (EIS) using the electrode polarization analysis. The structure of three of the SILLPs contains variable amounts of 1-butyl-3-methyl imidazolium chloride (BMIM[Cl]) strongly absorbed on the functional polymeric surfaces. The impedance spectra of the SILLPs show different ionic conductivity processes at different regions of the spectra. At higher frequency, the high conductivity observed is associated to the bis-((trifluoromethyl)sulfonyl)imide) (NTf_2^-) anion mobility. The ionic conductivity of SILLPs is increased up to 3 orders of magnitude in the presence of BMIM[Cl]. In this case, the highest ionic conductivity obtained was 2.56×10^{-3} S/cm at 30ºC and 1.3×10^{-2} S/cm at 80ºC. The experimental results show than the variation of ionic conductivity with the temperature is of VFT type. From the maximum loss tangent the inverse of Debye length has been obtained being 100 times higher when free bulk BMIM[Cl]is absorbed into the polymeric matrix. Finally the electrode polarization analysis overestimates the free ion diffusivity while underestimates the free ion number density.*

Keywords: Supported ionic liquids, ionic conductivity, imidazolium, electrochemical impedance spectroscopy (EIS).

***Corresponding author.** Departamento de Termodinámica Aplicada. ETSII. Universidad Politécnica de Valencia. C/Camino de Vera s/n. 46022. Valencia (Spain). Tel.: +34 96 387 93 28; Fax: +34 96 387 79 24. E-mail address: vicommo@ter.upv.es

1. Introduction

Ionic liquids (ILs) are organic compounds with a melting temperature below 100ºC with tendency to form supercooled melts. They have interesting physical properties such as their very low vapor pressure, high conductivity and very good thermal and chemical stability, which provide them a great potential as designer solvents for catalytic and chemical applications such as electrochemical membranes for capacitors, lithium-ion batteries, fuel cells and electromechanical transduction devices for actuators and sensors.[1-7] Ionic liquid structures can be incorporated into crosslinked macromolecular structures by physical entrapment to give rise to the so-called Supported Ionic Liquid Phases (SILPs),[8,9,10] or by covalent attachment affording Supported Ionic Liquid-Like Phases (SILLPs)[11]. Alternatively, linear Polymerized Ionic Liquids (PILs) can be prepared by polymerization of the corresponding functional monomers containing IL fragments.[12-14] Interestingly, the incorporation of IL fragments into polymeric matrices allows an efficient transfer of the intrinsic properties of the ILs to the polymeric surfaces, which is highly remarkable in the case of SILLPs with covalently attached moieties.[15,16] Through this approach, the physical properties of the resulting materials can be significantly altered by modifying the chemical structures of the constituent ions or the chemical or morphological properties of the polymeric backbone. This allows combining the inherent properties of ionic liquids with the consistency and mechanical properties of the supporting polymers affording new materials and composites with a high potential in electrochemical applications.[17-20]

A large number of examples can be found in the literature on the use of ILs and poly(ionic liquids) or PILs as electrolites.[21] In most cases, however, the examples considered involve using linear PILs, which can be considered beneficial in terms on ion mobility and, accordingly, conductivity. However, the use of linear (soluble) PILs has some disadvantages for specific applications requiring a strong mechanical strength, the achievement of specific shapes and morphologies (e.g. controlled porosity), high thermal stability and so on. In this regard we have followed an innovative approach with the preparation of monolithic polymers that can be designed at will in terms of their chemical composition, morphology, porosity or other properties, providing a simple scaffold for a variety of potential Supported Ionic Liquid-Like Phases (SILLPs) with a large set of applications of industrial interest.[11] Of course, the use of highly crosslinked

polymeric matrices reduce the mobility of the polymeric chains containing the IL-like fragments and this is accompanied by a decrease in conductivity. In our case, initial studies with SILLPs containing Cl^- as counter anions have revealed that the ionic conductivity drops significantly to values below 10^{-6} S cm^{-1} at room temperature, due to the decrease in the number of the mobile ions. However, it was also observed how this parameter increases about two orders of magnitude when the Cl^- counterion is exchanged by the NTf_2^- anion in such highly crosslinked poly (styrene-co-divinylbenzene) matrices.[19] The polymerization of a monomer bearing an ionic liquid-like fragment in the presence of an appropriate crosslinking agent and a room temperature Ionic Liquid (RTIL) represents a useful alternative to improve this situation.[20-22] This provides a polymeric backbone containing covalently attached IL-like moieties to which the IL molecules will be strongly associated. This approach can allow combining the advantages found for the two possible alternatives to supported ILs and eliminating, or at least minimizing, the potential leaching of the bulk IL phase. Besides, the resulting properties of these composites, in particular their conductivity, can be tailored by the proper selection of the polymeric and liquid components, in particular by a selection of the elements defining the interaction between the different IL-based subunits (anions and cations). Composites of ILs and PILs have been also studied previously, though they present some drawbacks similar to the ones considered for PILs and, besides, the potential leaching of the IL represents a serious limitation for their practical use, considering different factors including long-term applicability, cost issues and the environmental impact. These drawbacks are not present in our case as leaching seems to be absent under a variety of conditions.

In this work we have studied by impedance spectroscopy the ionic transport of five different SILLPs containing covalently attached 1-butyl imidazolium fragments and different loadings of 1-butyl-3-methyl imidazolium chloride as the RTIL component. We have considered the macroscopic polarization of mobile ion charges and free ion charges. Also, following the Trukham model[23] we are calculated, from the maximum in loss tangent positionated at moderate and higher frequencies, the values of the free ion diffusivity and we are estimate the values of ionic concentration of free charge carriers in the range of temperatures compress between 20ºC and 120ºC. The results presented demonstrate that the preparation of composites based on highly crosslinked SILLPs and bulk ILs allows to achieve conductivities comparable to those attained with bulk ILs but with the technological advantages associated to a solid material with a high mechanical

and thermal stability and that can be easily tuned to obtain the desired composition, shape and properties.

2. Experimental

2.1. Materials

1-Butyl-3-methyl imidazolium chloride (BMIM[Cl]), 1,1,1-tris-(hydroxymethyl)-propan-trimethacrylate (TMPTMA) (CAS: 3290-92-4), polyethylene glycol dimethacrylate (PEGDMA, CAS: 25852-47-5) and azobisisobutyronitrile (AIBN) were obtained from commercial sources and used without further purification. The liquid monomer **1** (VBIM[NTf2], 1-(4-vinylbenzyl)-3-butyl imidazolium bistriflamide) was synthesized following the procedure previously described.[24]

2.2. General procedure for the synthesis of the films F1-F5

A mixture of VBIM[NTf_2] **1**, the corresponding crosslinking agent (PEGDMA **2** or TMPTMA **3**), a 1 wt % of AIBN (as the initiator) and, when appropriate, BMIM[Cl] (**4**) was stirred and ultrasonicated to obtain a homogeneous solution. This solution was then cast into a glass mold by its introduction in the narrow space created between two microscopy slides separated by three thin lamellas and polymerization was carried out in an oven for 24 h at 65 °C. After cooling, the films were removed from the mold and washed several times with different organic solvents. The selected resulting polymers were homogeneous, transparent and ca. 4-5 cm x 1.5-2 cm in size, with thicknesses ranging from 375 to 590 µm. Nitrogen elemental analysis was used to obtain the final IL-loading of the polymers. In all cases, the experimental nitrogen percentage obtained was in good agreement with the expected values. The weight percent composition of the different mixtures used and the individual thicknesses are given in Table 1. For polymers F3-F5, no leaching for the bulk BMIM[Cl] was observed even after shoxlet extraction with organic solvents.[16,20] The same shoxlet extraction experiment, along with spectroscopic and elemental analysis data, allowed to confirm that a full polymerization of the monomeric mixture had taken place in all cases, with the absence of any monomer or oligomer in the extraction solvent at the end of the process.

2.3. Electrochemical impedance spectroscopy measurements

Impedance measurements were carried out on the polymeric films at several temperatures lying in the range 293 K (20ºC) to 393 K (120ºC) and within the frequency window $10^{-1} < f < 3x10^{6}$ Hz. The experiments were performed with 100 mV amplitude, using a Novocontrol broadband dielectric spectrometer (Hundsangen, Germany) integrated by a SR 830 lock-in amplifier with an Alpha dielectric interface. The sample of interest was sandwiched between two gold circular electrodes of 20 mm of diameter coupled to the impedance spectrometer acting as blocking electrodes. The membrane-electrode assembly was annealed in the Novocontrol setup under an inert dry nitrogen atmosphere previously to the start of the actual measurement. For this, firstly two temperature cycles (20-120-20ºC) were carried out in 10ºC steps. At the third scan of temperature, the dielectric spectra were collected for each step. This was performed to ensure the measurements reproducibility and to avoid the interference from humidity that could be adsorbed onto the corresponding materials. During the measurements, the temperature was maintained (isothermal experiments) controlled by a nitrogen jet (QUATRO from Novocontrol) with a temperature error of 0.1 K during every single sweep in frequency. Before and after the experiments the thickness of the sample was measured by a micrometer, observing that in all the cases the thickness did not appreciably vary (±20μm, less than 5%).

3. Results and discussion

The synthesis of the different polymeric films (**Figure 1**) was carried out by radical polymerization at 65ºC during 24 h of monomeric mixtures based on the styrenic monomer containing imidazolium fragments **1**. The polymerization took place in a glass mold formed by two glass slides separated by three cover slips. Two different crosslinking agents and different crosslinking degrees were considered in order to obtain insoluble polymers displaying simultaneously good permeability and mechanical strength. For films **F1-F3** the crosslinker was poly(ethylene glycol) dimethacrylate (PEGDMA, **2**). The corresponding polymeric matrices differed on the degree of crosslinking associated to the content of **2** in the monomeric mixture (from 10 to 20% in weight), and film **F3** was obtained in the presence of an additional IL-phase BMIM[Cl]. Samples **F4**

and **F5** were obtained in the presence of a trifunctional crosslinking agent like trimethylolpropane trimethacrylate (TMPTMA, **3**). This allowed the preparation of mechanically stable films with low crosslinking degrees (≤ 10 %) and a high content in the bulk IL phase (45-47 % of **4**). In this case, and as a proof of concept of the validity of our approach, we have only considered two anions for the IL-fragments: Cl^- and NTf_2^- as representatives of two separated families of anions in ILs (highly coordinative anions giving place to polar hydrophilic ILs and poorly coordinative anions giving place to less polar and more hydrophobic ILs). Moreover the initial selection of these two anions is supported by other additional factors like their reduced cost (of interest for practical applications), their high stability under a variety of conditions (precluding incorrect measurements associated to the decomposition of the anion) and their lower environmental impact in case of leaching and release to the environment.

After demolding, only those films being transparent and mechanically stable, being ca. 4-5 cm x 1.5-2 cm in size, were retained for further studies. Polymers **F1-F3** containing PEGDMA (**2**) as the crosslinker presented a thickness of about 390 ± 15 μm, while polymers **F4** and **F5** containing TMPTMA (**3**) displayed thicknesses of about 580 ± 10 μm. The exact thickness and composition for each individual film is presented in **Table 1**. All the prepared polymers displayed the expected elemental analyses and spectroscopic properties.[15,16,19,20] The FT-IR and FT-Raman spectra confirmed the presence of the expected functionalities. Thus, the absence of any band at 1630 cm^{-1} that can be assigned to the residual unreacted double bonds indicates the full incorporation of the monomeric components into the final polymer. The bands corresponding to the presence of the imidazolium units (e.g. 3153, 3147, 1388, 1189, 627 and 606 cm^{-1}) are clearly visible. The presence of the NTf_2^- anion is easily visualized through the intensity of the O=S=O stretching band at ca. 1189 cm^{-1}. The presence of Cl^- instead of NTf_2^- cannot be monitored as it is just associated to minor shifts in the frequencies of the bands associated to the more acidic C-H groups in the imidazolium fragment.[25]

Figure 1.

Table 1.

Impedance spectroscopy measurements were carried out for the samples **F1**-**F5** at different temperatures in order to obtain the conductivity, the diffusion coefficient and the density of ionic charge carriers. The electrical conductivity σ can be obtained from the imaginary part of the complex dielectric permittivity (ε*=ε'–jε") where ε"= σ/(ε_0 ω), being ε_0 the permittivity of vacuum and ω the angular frequency of the applied electric field. The plot of log ε" versus log ω on the high frequency region permit us observe that the imaginary part of the permittivity increase with decreasing frequency as ε"~ ω^{-1}, exhibing a straight line with slope practically equal to -1.The extrapolation where log ω=0 determine the normal behavior of direct current conduction and then the dc-conductivity (σ_{dc}) is obtained.

On the other hand, in this region the Nyquist diagrams -Z" (imag.) vs Z'(real) are semicircles intersecting the abscissa axis in the high frequency region at Z'=R_0. This value also represents the dc-conductivity. Both methods were followed to obtain the dc-conductivity of the samples. Departure from semicircles is observed experimentally as a result of polarization processes and other possible phenomena taking place at the membrane electrode interface. As it is known, polarization processes in condensed matter are not defined by a single relaxation time, but through a distribution of relaxation times, τ_i. The impedance behavior of these complex systems can be analyzed by an equivalent circuit, made up of a polarization resistance R_{pi}, in parallel with a constant phase element (CPE) according to the expression CPE= $1/(j\omega C)^n$, where , j is the imaginary unit (j^2= -1), *n* is a frequency independent parameter lying in the $0<n<1$ range, ω ($=2\pi f$) is the angular frequency and C is a CPE-parameter which represents the differential capacitance of the interface when n=1, a resistor when n=0 and a inductor in case of n=-1. However, when n<1 C cannot represent the capacitance because its unities are not simple Farads[26]. In some cases these systems combine polarization processes with a frequency independent resistance, or ohmic resistance, R_0. In such a case, the equivalent electrical circuit can be given by a series of R-CPE parallel circuits in series with R_0. This is represented in the insets of **Figure 2** for each sample[27]. The impedance of the circuit is given by

$$Z^*(\omega) = R_0 + \frac{1}{(j\omega C)^n} + \sum_i \frac{R_{pi}}{1+(j\omega\tau_i)^{a_i}} \qquad (1)$$

Notice that for a_i= 1, the eq. (1) corresponds to the complex impedance of a Debye system. It is worth noting that the Nyquist plot[28] (-*Z*" vs *Z*' plots), converge to $Z'=R_0$ at $\omega\to\infty$ and $Z'=R_{pi}$ at $\omega\to 0$, independently on the value of *n* and a_i. In Figure 2 we can see the Nyquist plot for all the samples, at 20ºC. In the same figure, the insets allow to observe the dependence of the conductivity with the frequency at 20ºC. From the intercept in the abscissa axis we can determine the dc-conductivity as

$$\sigma' = \frac{L}{R_0 \cdot S} \qquad (2)$$

As we can see from **Figure 2**, the samples **F1** and **F2** displayed a single arc, but the samples **F3**, **F4** and **F5**, exhibited two arcs that can be associated to the presence of two different conductive processes in the films, each one having a characteristic conductivity. The conductivity values found at 20 and 40ºC were in agreement with the equivalent circuits shown in the inset of each figure and are gathered in **Table 2**. Alternatively, the Bode diagrams obtained for the same samples, at 20ºC and 30ºC, are shown in **Figure 3**. This figure reveals that the real part of the conductivity increases with the frequency and tends to a constant value when the phase angle, φ, reaches a maximum for each temperature. As can be seen for the samples **F1** and **F2**, all the Bode diagrams showed a plateau when plotting σ' *vs* frequency in the region of moderate frequencies (10 to1000 Hz), coexisting with the peak of the phase angle. However, for the sample **F3**, the plateau was observed in the region of 10^3 to 10^5 Hz and for the samples **F4** and **F5** the plateau is even displaced at higher frequencies (between 10^4 and 10^6 Hz) coexisting with the peak of the phase angle, φ, tending to zero value. On the other hand, for samples **F3**, **F4** and **F5**, in the region of moderate frequencies (10-100 Hz), a second plateau was observed for the real part of the conductivity at the region where the phase angle reaches a less pronounced maximum, at -10º, -20º and -30º, respectively for the three samples. The values of the real part of the conductivity when the peak of phase angle reaches a maximum value were practically identical than the ones obtained from Nyquist diagrams and the intercept of the straight line of log ε'' versus log ω in the region with the slope being -1. Therefore these values were taken as

the dc-conductivity of the samples, σ_{dc}, and the values obtained for the 20 ºC - 50ºC temperature range are given in table 3.

Table 2.

Figure 2.

Figure 3.

The existence of two types of processes corresponding to the mobilities of the two anions present in samples **F3**, **F4** and **F5,** was detected from both Nyquist and Bode diagrams (see **Figures 2** and **3**, respectively). This can be attributed to the existence of different conductive processes related with the nature of the ions present in the polymeric matrix. Thus, each ion can contribute in diverse ways to the motions within the material, depending on its shape and size, providing different mobility and diffusion coefficients.

Previous studies carried out with other SILLPs in the presence of anions like NTf_2^- or Cl^- have shown that the NTf_2^- anions show a higher ionic conductivity than Cl^- ions.[19,20,29,30] As mentioned above, the NTf_2^- anion is present in all studied SILLPs and, therefore, we can identify the ionic conductivity of **F1** and **F2** with the mobility associated to this anion. However for the SILLPs **F3**, **F4** and **F5** the ionic conductivity observed at moderate and high frequencies will be associated to both $NTf_2^-$and Cl^- anions and then two different conductivities, mobilities and diffusion coefficients will be present. The dc-conductivities obtained from Bode diagrams for all the samples are gathered in **Table 3**.

Figure 4.

The dependence of the loss tangent as a function of the perturbation frequency, at 20ºC and 30ºC, are represented for all the samples in **Figure 4**. As can be seen, when the temperature increased, the frequency of the maximum value shifted to higher values. As seen in the Nyquist and Bode diagrams, (**Figures 2** and **3**) and also in **Figure 4**, only one process associated with the dc-conductivity could be observed for the samples **F1** and **F2**. However, two different peaks were observed at moderate and high frequencies, associated with two different processes, for the samples **F3**, **F4** and **F5**. Both processes are due to presence of the additional IL-phase 1-butyl-3-methyl imidazolium chloride (BMIM[Cl]) incorporated to the polymeric matrix obtained by the full polymerization of VBIM[NTf_2]. The value of the frequency at which *tan* δ reached the maximum was consistent with the plateau of the real part of the conductivity in the Bode diagram. This value, (f_{max}(tan δ)), was taken as the frequency which permits to obtain the dc-conductivity of the samples (σ_{dc}). This frequency is related with the electrode polarization (EP), and can be used to analyze the free charge density and the diffusivity following the procedure described previously.[23,24,26,30-38] In **Figure 3**, the arrows indicate the onset of EP as the minimum in the plot of the complex conductivity (σ") and the full development of EP as the maximum observed in the same plot of (σ").[35-40]

On the other hand, **Figure 3** showed that with the increase in frequency the conductivity only increased one order of magnitude for the samples with a significant amount of adsorbed ionic liquid phase (**F3**, **F4** and **F5**), but about two orders of magnitude in the case of the samples containing only covalently attached IL-like fragments (**F1** and **F2**). This could be observed for a wide range of temperatures (30-120°C). The ionic conductivities observed at lower frequencies, having a phase angle below 0°, revealed that other phenomena associated with the ionic conductivity were masking the true ionic conductivity expected for the ionic liquids. Such phenomena have been related with capacitance effects that correspond to the charge accumulation due to the macroscopic Debye polarization, the dipole orientation, blocking electrodes and the existence of impurities.[31-34] They are observed mainly in the low frequency range where the interfacial polarization at the condenser plates cooperate with the Maxwell-Wagner-Sillars (MWS) effect.[31-40] Obtaining the true contribution of each ion to the ionic transport in polymerized ionic liquids and mixtures formed between ILs and molecular liquids (ML) is very difficult. To achieve this, it is necessary to know the respective roles of the cations and anions in the samples from conductivity measurements. As the

conductivity is obtained for the complete system, it represents the sum of the total contributions of the mobile charges, i.e., $\sigma = \sigma_+ + \sigma_-$.[41] In studies to measure the diffusivity of ILs in polymerized ionic liquids (PILs) using the method of pulsed field gradient (PFG) NMR measurements, it has been observed that the conductivity of the PIL is greater than that of its molecular counterpart.[41] This indicates that the cation mobility is very slow to provide a significant contribution to the true conductivity of the samples that can be dominated by the contributions of the free anions. Thus, although all the available charges participate in the ionic transport, it can be assumed that the highest contribution to the true conductivity, $\sigma = \sigma_{dc}$, for all the samples will be the mobility of the anions. The values of conductivity obtained for each of the samples for the whole range of temperatures studied are given in **Table 3**. A close inspection of this table shows that the dc-conductivity increased with the temperature as a consequence of the thermal activation process.

Table 3

As can be seen in **Figure 3**, the presence of the adsorbed ionic liquid BMIM[Cl] in the matrix of SILLPs **F3**, **F4** and **F5** increased the ionic conductivity at high frequencies between 1.5 (**F3**) and 3 orders of magnitude (**F4** and **F5**) relative to the related polymers **F1** and **F2** lacking the adsorbed phase. Clearly, the higher proportion of adsorbed IL (BMIM[Cl]) in SILLPs **F4** and **F5** over **F3** resulted in a further increase in ionic conductivity. An analysis of the variation of the conductivity with the temperature can be obtained from the Arrhenius plot shown in **Figure 5**, where log σ_{dc} is represented *versus* the reciprocal of the absolute temperature for all the samples studied.

Figure 5.

Figure 5 shows that the data display a Vogel-Fulcher-Tamman (VFT) type behavior, which is typical for the majority of polymers at temperatures above transition temperature (T_g). For all the temperatures studied, the values of the conductivities obtained increased with the temperature, following the trend σ(**F5**)> σ(**F4**)> σ(**F3**) >

σ(**F2**)~ σ(**F1**). As observed in **Figure 5**, the dc-conductivity was associated to the higher mobility of the polymeric chains and the adsorbed ILs as well as to the increase in the loading of IL-like fragments covalently attached to the polymeric matrix.

For example, at 30ºC the values of the conductivities were $1.24x10^{-7}$ S/cm, $1.30x10^{-7}$ S/cm, $6.1x10^{-5}$ S/cm, $1.6x10^{-3}$ S/cm and $2.6x10^{-3}$ S/cm, for **F1**, **F2**, **F3**, **F4** and **F5**, respectively. Thus, the addition of 16% in weight of the adsorbed IL in **F3** produced an increase of about 2.5 orders of magnitude in the conductivity, for all the studied temperatures, with respect to the samples **F1** and **F2** not containing any bulk IL. However, as commented before for the Nyquist and Bode diagrams, the samples **F3**, **F4** and **F5** containing two kinds of anions (NTf_2^- and Cl^-), showed two different processes associated to the corresponding conductivities, as seen in **Figures 2**, **3** and **4**. A general comparison between all the samples for the whole range of temperatures showed, for instance, that the dc-conductivity associated to the Cl^- ion in **F5** sample increased from $1.6x10^{-3}$ S/cm at 20°C to $2.4x10^{-2}$ S/cm at 120°C, while in case of the **F4** sample this increase was from $1.0x10^{-3}$ S/cm to $1.8x10^{-2}$ S/cm for the same temperature range. The slight increase observed in **F5** respect to **F4** may be due to the small increase in IL loading in **F5** and the change in crosslinking, which is also slightly lower in **F5**. However, the conductivity associated to the NTf_2^- ions, which are the only ones present in samples **F1** and **F2**, varied, respectively, from $3.0x10^{-7}$ S/cm to $3.1x10^{-4}$ S/cm and from $3.0x10^{-7}$ S/cm to $5.3x10^{-4}$ S/cm for the same interval of temperatures. In this case, the conductivity did not increase significantly for **F2**. Only at high temperatures some small differences were detected. Overall, the results show that a huge increase in conductivity, in particular at low temperatures (up to 4 orders of magnitude) can be obtained through a proper selection of the different components and structure of the corresponding SILLPs. Our results show that the ionic conductivity of these materials is comparable or higher than those reported for related systems, reaching an ionic conductivity of 10^{-3} S/cm at 30ºC. In the case, for instance, of a linear ABA triblock copolymer poly(styrene-b-[1-ethyl-3-(4-vinylbenzyl)imidazolium bis(trifluoromethane sulfonyl)imide)]-b-styrene) a value of *ca*. $5x10^{-7}$ S/cm was observed around 40 ºC, reaching a maximum measured value of about $3x10^{-4}$ S/cm around 150 ºC.[17] For the non-crosslinked benchmark PIL poly(1-vinyl-3-ethylimidazolium) [NTf_2] different studies have reported values of $6.3x10^{-7}$, $2.5x10^{-11}$ and $5.0x10^{-5}$ S/cm at 20-30 ºC.[27] In the case of ion gel materials recently reported, values of $1.3x10^{-4}$ S/cm were found at 25ºC.[42]

The fit of the values represented in the Arrhenius plot of **Figure 5** to a Vogel-Fulcher-Tamman (VFT) equation, allows obtaining the temperature dependence of the dc-conductivity according to eq. (3).

$$\ln \sigma_{dc} = \ln \sigma_{\infty} - \frac{B}{T - T_0} \qquad (3)$$

In this equation, *B* is a fitting parameter related with the curvature of the plot that can be seen as the high temperature activation energy of the process underlying the conductivity (σ_{dc}). T_0 is the Vogel temperature, considered as the one at which the relaxation time would diverge and σ_{∞} is a pre-factor related with the conductivity limit at higher temperatures. **Table 4** gathers the corresponding values obtained for the parameters $ln\sigma_{\infty}$, T_0 and *B*. In the same table the values found for the activation energy have also been tabulated. On the other hand, the χ^2 values, corresponding to the sum of the squared deviations between the logarithmic values of conductivities obtained from the fitting and the experimental ones, are also given being small in all cases.

Table 4.

The values obtained for the activation energies associated to the conductivities of the different samples followed the order **F2>F1>F3>F4>F5**. It is worth mentioning that a decrease in the crosslinking, with the associated increase of the IL-like fragments loading, in **F2** as compared to **F1**, produced an increase in the activation energy. This suggests the presence of strong intrapolymeric interactions between the ionic fragments, facilitated by higher degrees of functionalization and lower crosslinking degrees, which finally can impart more rigidity to the matrix. This is reflected in experimental observations like the higher fragility of the polymer and the increase in the activation energy for **F2** and can explain the small differences observed in conductivity between **F1** and **F2** in spite of the higher ionic loading of **F2**. A similar phenomenon can justify that **F4** and **F5** show E_{act} values that are quite similar between them but smaller than for **F3**. The introduction of significant amounts of Cl^- in samples **F4** and **F5** can also be important in this regard, taking into account the higher coordinating ability of this anion.[25]

Diffusion coefficients and charge concentration of ions.

The more important parameters to characterize and estimate the ionic transport in polymers and membranes are the mobility and the total charge carrier concentration. However, they are in general difficult to quantify. There are a great number of alternative approaches for determining these parameters under the application of an electric field.[19-23,30-55] Some of them use a generalization of the theory of Trukhan[23] following the Nernst-Planck electrodiffusion equations linearized for the dielectric dispersion caused by the electrodiffusion of ions in a polymeric membrane charged and confined between two electrodes.[31-33] To give an estimation of the diffusivity and the free mobile ion from the dielectric spectra we have considered this model based on the analysis of the dielectric spectra of the electrode polarization. From this analysis the average free ion diffusivity concentrations has been calculated as[31-36]

$$D = \frac{\omega_{\max}^{\tan\delta} \cdot L^2}{32\left(\tan^3\delta\right)_{\max,\omega}} \cdot \qquad (4)$$

where $\omega_{\max}^{\tan\delta}$ is the angular frequency corresponding to the peak in the loss tangent, $(\tan\delta)_{\max,\omega}$ its value at this frequency $(\tan\delta)_{\max}$, and L, the sample thickness

Figure 6 shows the experimental values for *tan* δ as a function of the perturbation frequency. It can be observed that the peak corresponding to the maximum of *tan* δ shifted towards higher frequencies as the temperature increased for all the samples. However, at low frequencies, a second peak of lower intensity was observed and this can be related with the interfacial polarization due to the participation of other ions. Previous works from our group,[20-23] have shown that dynamical electric double layers, described by means of Nernst-Planck-Maxwel electrodynamics, produce an excess of impedance in addition to the MWS impedance, and the combined effect of both impedances is the apparition of a maximum in *tan* δ , since the real part of the permittivity, ε', rises when increasing the frequency as a reflection of the capacitance of the macropolarization, that in our case could be due to NTf_2^- and Cl^- ions. A close inspection of the graphs in **Figure 6** shows that samples **F3**, **F4** and **F5** displayed peak heights much larger than samples **F1** and **F2**, not containing the additional BMIM[Cl]. On the other hand, the samples prepared by the polymerization of VBIM[NTf_2] as the only ionic component presented more symmetric peaks whose height decreased with the

increase in NTf_2^- loading, possibly due to the higher elasticity associated to the higher level of PEGDMA.

Figure 6

From the values plotted in **Figure 6** for the whole range of temperatures, the diffusion coefficients of the samples were determined by means of equation (4). The values found are plotted in **Figures 7a** (**F1** and **F2**) and **7b** (**F3**, **F4**, **F5**).

Figure 7

On the other hand, from **Figure 6** and knowing the thickness of the sample, L, the inverse of Debye length, κ, can be estimated, as[31-34]

$$(\tan\delta)_{\max,\omega} \approx \sqrt{\frac{\kappa L}{8}} \qquad (5)$$

Notice that the equation (5) is only valid in the case that $\kappa L >> 1$. The obtained values for this parameter (κL) are given in **Table 5**. For all the samples, the inverse of the Debye length followed the trend κ(**F2**)< κ(**F1**)< κ(**F3**)< κ(**F4**)~ κ(**F5**) at 20ºC, varying from about of $8.5x10^{-7}$ m^{-1} for **F2**, for which only the covalently attached IL-fragment containing the NTf_2^- anion is present, to $2.6x10^{-5}m^{-1}$ in the case of **F4** and **F5** also containing free BMIM[Cl] incorporated into the polymeric matrix. This behavior is in agreement with the variation of the conductivity and activation energy associated to this parameter.

Table 5

Taking into account the Einstein relation and knowing the conductivity and diffusivity, values calculated as described above, the free-ion number density, *n*, could be obtained by mean of the expression:

$$n = \frac{k_B T}{q^2} \frac{\sigma}{D} \qquad (6)$$

Here k_B is the Boltzmann constant, *T* the absolute temperature, *q* the amount of charges carried by an ion, σ the dc-conductivity, ($\sigma = \sigma_{dc}$), of the samples, and *D* the average free ion diffusivity. The equation (6) allowed determining the average concentration of charge carriers from the values of the ionic conductivity previously measured (**Table 3**) and from the values of diffusion coefficients determined according to equation (4)(**Figure 6**). In **Figure 8** the estimated free ion concentration values for each of the samples are collected, assuming the electrolyte to be univalent, as a function of 1000/T. A close inspection of **Figure 8** shows that the free ion number density decreased at lower temperatures for all the samples. However, the presence of the free BMIM[Cl] produced an increase in the ionic charge density. A comparison between **F3** and **F4** reveals that the increase from 16% to 45% in the amount of bulk IL was accompanied by an increase of the ionic charge density of about two orders of magnitude at all temperatures. Similarly, a comparison between the samples **F2** (without bulk IL) and **F3** (with 16% of bulk IL) revealed an increase in the density for **F3** of about one order of magnitude, in spite of the fact that the total amount of imidazolium subunits is very similar in both cases. Finally, the comparison of the samples **F1** and **F2** indicated a reduction of the ionic mobile charge density in **F2** although the amount of initial VBIM[NTf_2] in the monomeric mixture increased from 80% to 90%. This agrees with the former suggestion that an increase in the IL-like fragments loading and a decrease in the amount of PEGDMA favors intra polymeric ion-ion interactions and provides a more rigid final polymer.

Figure 8

Our analysis based on electrode polarization gave a quantity of free ion concentration, *n*, lower than the total amount calculated theoretically, n_{tot}, being evident that these results overestimated the ion diffusivity. In general, the free ion concentration can be described by the Arrhenius equation $n=n_0 \exp(-E_{dis}/k_BT)$, where E_{dis} is the dissociation energy and n_0 the number density in the high temperature limit at which we can assume a complete dissociation. As it is known the electrode polarization model is based on the Debye-Hückel theory and therefore can be expected that this model fails in the case of high ionic concentrations. To solve this contradiction, we have followed the same line of reasoning that Wang et al.[35,36], correcting the number density using the factor of proportionality, $N = \frac{n_{tot}}{n_0}$ and its reciprocal $\frac{1}{N} = \frac{n_0}{n_{tot}}$ to correct the diffusivity. In this case n_{tot} is the total ion number density calculated theoretically from the preparation of the samples. In this way the corrected diffusivity will be

$$\tilde{D} = D\frac{n_0}{n_{tot}} \qquad (7)$$

where $\tilde{D}$, is the diffusivity after correction and *D* is the value obtained from the maximum in loss $tan\ \delta$ following the generalized model of Trukhan[23] by means of eq. (4).

Figure 7 shows the corrected and uncorrected free ion diffusivities. As can be seen, the uncorrected diffusivities calculated from the EP model were two or three orders of magnitude higher than the corrected values. This result revealed that polymers containing both covalently attached and absorbed ionic liquid fragments (like **F1**, **F2** and **F3**) can provide even stronger decoupling of ionic conductivity and higher conductivities than flexible ionic polymers. Similar results have been observed in other polymers with ionic salts incorporated such as PEO or PVC-PPEOMEMA/LiTFSI.[35,36]

Finally, assuming that the mobility is only associated to the contribution of the anions, the conductivity (σ_{dc}) of the samples for each one of temperatures was obtained and the values of the inverse Debye length could be determined from the peaks of the loss tangent using the eq. (5). The values of the static permittivity, ε_s, ($\varepsilon' \rightarrow \varepsilon_s$ for $\omega \rightarrow 0$), also named as bulk permittivity could be estimated as[14]

$$\varepsilon_s = \frac{2 \cdot \sigma_{dc} \cdot \tau_{EP}}{\varepsilon_0 \cdot \kappa L} \qquad (8)$$

where, ε_0 is the permittivity of vacuum. At low frequencies the conducting ions begins to polarize at the electrodes and then the time scale for conduction becomes diffusive and the effective permittivity, after EP is complete, is given by

$$\varepsilon_{EP} = \frac{\sigma_{dc} \cdot \tau_{EP}}{\varepsilon_0} \qquad (9)$$

From eqs. (8) and (9) the values of the static permittivity and effective permittivity at 20 and 50ºC were calculated and the results are gathered in **Table 5**.

A close inspection of this table shows that the presence of the absorbed BMIM[Cl] produced an increase in the static permittivity. In the case of the samples containing only covalently attached IL-like fragments, as is the case of **F1** and **F2**, the values achieved were of the same order of magnitude than the ones reported by Choi et al. for imidazolium acrylates and methacrylates and their ionomers where ε_s was up to 140 at room temperature.[14b] After polymerization, the ε_s of the samples containing free BMIM[Cl] absorbed on the polymeric matrix (**F3**, **F4**, **F5**) were 3 to 5 times higher than in the case of polymers just containing covalently attached IL-fragments (**F1**, **F2**).

4. Conclusions

A deep study of the ionic transport in five SILLPs samples has been carried out by impedance spectroscopy. Three of the samples contain 16%, 45% and 47% of bulk BMIM[Cl] (over the total weight of the films) adsorbed on the polymeric matrix (**F3**, **F4** and **F5**, respectively) and also have covalently attached imidazolium subunits (65, 43 and 47 % in weight of VBIM[NTf_2] in the initial monomeric mixture). On the contrary, samples **F1** and **F2** do not possess any absorbed IL and the amount of covalently attached imidazolium fragments is 80 and 90 % in weight respectively (based on the amount of VBIM[NTf_2] in the initial monomeric mixture). Two different ion conduction processes have been observed for samples **F3**, **F4** and **F5** associated to NTf_2^- and Cl^- anions respectively, in comparison with samples **F1** and **F2**, where only one conductive process was observed. The conductivity of the considered polymeric materials increases up to three orders of magnitude when the bulk ionic liquid BMIM[Cl] is absorbed in the polymeric matrix at ambient temperature. The differences

can be ascribed, on the one hand, to the intra-cation and inter-cation hopping of the NTf_2^- anions, and on the other hand, to the free bulk IL (BMIM[Cl]) that is absorbed in the polymeric matrix.

The samples **F4** and **F5** reach an ionic conductivity of 10^{-3} S / cm at 20ºC, increasing this value one order of magnitude at 80ºC. The variation of ionic conductivity of the SILLPs displays a VFT behavior. The model used has also permitted obtaining the values of ion diffusivity and number density. For this kind of composite polymers containing both a high ion concentration of covalently attached fragments and absorbed free ILs in the matrix (BMIM[Cl]), the electrode polarization analysis overestimates the free ion diffusivity while underestimates the free ion number density. Therefore, the study of free ion diffusivity and number density from the generalized Trukhan model (electrode polarization model) must be considered with caution being of utility the corrections proposed by Wang et al.,[35,36] Finally, the model used has allowed obtaining the static permittivity, the effective permittivity after electrode polarization is complete and the film thickness scaled by the Debye length (κL) where κ is the inverse Debye length.

Acknowledgements

This research has been supported by the ENE/2011-24761 project, granted by the Ministerio de Economía y Competitividad (MINECO), Spain, and also by the grants CTQ2011-28903-C02-01 y PROMETEO2012/020.

References

1. Ionic Liquids. Topics in Current Chemistry 290, Barbara Kirchner (Editor), Springer, Heidelberg, 2009.
2. Green Solvents II. Properties and Applications of Ionic Liquids. Ali Mohammad, Inamuddin (Editores). Springer, Heidelberg, 2012.
3. Ohno, H. Electrochemical Aspects of Ionic Liquids; wiley-Interscience. J. Wiley: Hoboken, NJ, 2005.

4. Armand, M.; Endres,F.; Macfarlane, D.R.; Ohno, H.; Scrosati, B. Nat. Mater. 8 (2009) 621.

5. Xu, W.; Angell, C.A. Science. 297 (2002) 983.

6. Fernicola, A.; Scrosati, B.; Ohno, H.; Ionics. 12 (2006) 95.

7. Greaves, T.L.; Drummond, C. J. Chem. Rev. 108 (2008) 206.

8. Ueki, T., Watanabe, M. Macromolecules 41 (2008) 3739.

9. Lu, J., Yan, F., Texter, J. Progr. Polym. Sci. 34 (2009) 431.

10. Fehrmann, R., Riisager, A., Haumann, M. Supported Ionic Liquids: Fundamentals and Applications, Wiley-VCH, 2014.

11. a) Lozano, P., García-Verdugo, E., Piamtongkama, R., Karbass, N. , De Diego, T., Burguete, M.I., Luis, S.V. , Iborra, J.L. Adv. Synth. Catal. 349 (2007) 1077. b) Lozano, P., Burguete, M.I., Karbass, N., Montague, K., de Diego, T., Luis. S.V. Green Chem., 12 (2010) 1803. c) Burguete, M.I., García-Verdugo, E., Luis, S.V., Restrepo, J. Phys. Chem. Chem. Phys., 13 (2011) 14831. d) Izquierdo, D.F., Bernal, J.M., Burguete, M.I., Garcia-Verdugo, E., Lozano, P., Luis S.V. RSC Adv., 3 (2013) 13123. e) Martín, S., Porcar, R., Peris, E., Burguete, M.I., Carcía-Verdugo, E., Luis, S.V. Green Chem., 50 (2014) 1639.

12. Weber, R.L.; Ye Y.; Schmitt, A.L.; Banik, S. M.; Elabd, Y.A.; Mahanthappa, M.K. Macromolecules, 44 (2011) 5727.

13. Green, O.; Grubjesic, S.; Lee, S.; Firestone, M.A.; Polym. Rev., 49 (2009) 339.

14. a) Choi, U.H.; Le, M.; Wang, S.; Liu, W.; Winey, K.I.; Gibson, H.W.; Colby, R.H.. Macromolecules, 45 (2012) 3974. b) Choi U.H., Mittal A, Price L.T., Gibson H.W., Runt J, Colby R.H. Macromolecules, 46 (2013) 1175.

15. Burguete, M.I., Galindo, F., García-Verdugo, E., Karbass, N., Luis, S.V. Chem. Commun. 2007, 3086.

16. Sans, V., Karbass, N., Burguete, M.I., Compañ, V., García-Verdugo, E., Luis, S. V., Pawlak. M. Chem. Eur. J., 17 (2011) 1894.

17. (a) Yuan, J., Mecerreyes D., Antonietti, M. Progr. Polym. Sci., 38 (2013) 1009; (b) Yuan J., Antonietti, M. Polymer, 52 (2011) 1469; c) Green M. D., Long, T. H. E. Polym. Rev., 49 (2009) 291.

18. Luis, S. V., García-Verdugo, E., Burguete, M. I., Andrio, A., Molla S., Compañ, V. Polymers with Ionic Liquid Fragments as Potential Conducting Materials for Advanced Applications, in Applications of Ionic Liquids in Science and Technology, S. Handy Ed., InTech, 2011, Chapter 5. pp. 83-108.

19. Garcia-Bernabé, A., Compañ, V., Burgete, M.I., García-Verdugo, E., Karbass, N., Luis, S. V., Riande, E. J. Phys Chem. 114, (2010) 7030.

20. Altava, B.; Compañ, V.; Andrio, A.; del Castillo, L. F.; Mollá, S.; Burguete, M. I.; García-Verdugo, E.; Luis, S. V. Polymer, 72 (2015) 69.

21. Shaplov A.S., Marcilla R., Mecerreyes D. Electrochim Acta 175 (2015) 18.

22. Green, M. D.; Wang, D.; Hemp, S. T.; Choi, J.-H.; Winey, K. I.; Heflin, J. R.; Long, T. E. Polymer, 53 (2012) 3677.

23. Trukhan. E.M. Sov. Phys. Solid State (Engl. Transl), 4 (1963) 2560.24.

24. Tang, J., Tang, H., Sun, W., Plancher, H., Radosz M., Shen, Y. *Chem. Commun.*, 26 (2005) 3325.

25. González, L., Altava, B., Bolte, M., Burguete, M. I., García-Verdugo, E., Luis, S. V. Eur. J. Org. Chem., (2012) 4996.

26 Hirschorn, B., Orazem, M.E., Tribollet, B., Vivier, V., Frateur, I., Musiani. M. Electrochim Acta, 55 (2010) 6218.

27. MacDonald, J. R. Impedance Spectroscopy. Emphasizing solid materials and systems, Wiley-Interscience, 1987. b) Paddison. S. J. Annu Rev. Mat. Res. 33 (2003) 289.

28. Nyquist. H. Phys. Rev. 32 (1928)110.

29. Huber, B., Rossrucker, L., Sundermeyer, J., Roling, B., Solid State Ionics, 247-278, (2013) 15.

30. Compañ, V., Molla, S., García-Verdugo, E., Luis, S.V., Burguete, M.I., J. Non-Cryst. Solids. 358 (2012) 1228.

31. Sorensen, T. S., Compañ, V. J. Chem. Soc., Faraday Trans., 91 (1995) 4235.

32. Sorensen, T. S., Compañ, V., Diaz-Calleja. R. J. Chem. Soc., Faraday Trans., 92 (1996) 1947.

33. Compañ, V., Sorensen, T. S., Diaz-Calleja R., Riande, E. J. Appl. Phys., 79 (1996) 403.

34. Munar, A., Andrio, A., Iserte, R., Compañ, V. J. Non–Cryst. Solids 357 (2011) 3064-3069.

35. Wang, Y., Su, Che-Nan, Fan, F., Sangoro, J.R., Berman, M.B., Grenbaum, S.G., Zawodzinski, T.A., Sokolov, A. P. Physical Review E 87 (2013) 042308.

36. Wang, Y., Fan, F., Agapov, A. L., Sait, T, Yang, J., Yu, X., Hong, K., Mays, J., Sokolov, A. P. Polymer 55 (2014) 4067.

37. Macdonald J.R. J. Phys.: Condens. Matter 22, (2010) 495101

38. Macdonald, J.R., Evangelista, L.R., Lenzi, E.K., Barbero G. J. Phys. Chem. C 115 (2011) 7468.

39. Klein, R. J., Zhang, S., Duo, S., Jones, B. H., Colby R. H., Runt, J. J. Chem. Phys., 124 (2006) 144903.

40. Bandara, T.M.W.J., Dissanayake, M.A.K.L., Albinsson, I., Mellander, B.-E. Solid State Ionics, 189 (2011) 63.

41. Kunal, K., Robertson, C.G., Pawlus, S., Hahn, S.F., Sokolov, A.P. Macromolecules 41 (2008) 7232.

42. Shaplov, A.S., Ponkratov, D., Vlasov, P., Lozinskaya, E. et al., J. Mat. Chem. A, 3 (2015) 2188.

43. Dudowicz, J., Freed, K.F., Douglas, J.F. J. Phys. Chem B 109 (2005) 21285-

44. Maxwell, J.C. A Treatise of Electricity & Magnetism, Dover, New York, 1954, Articles 310-314.

45. Leys, J., Rajesh, R.N., Menon, P. C., Glorieux, C., Longuemart, S., Nockemann, P., Pellens, M., Binnemans, K. *J. Chem. Phys.*, 133 (2010) 034503.

46. Watanabe, M., Nagano, S., Sanui, K., Ogata. N. Solid State Ionics, 911 (1988) 28.

47. Hayamizu, K., Akiba, E., Bando, T., Aihara. Y. J. Chem. Phys., 117 (2002) 5929.

48. Agrawal, R.C., Kumar, R., Gupta. R.K. Materials Science and Engineering, B57 (1998) 46.

49. Niklasson, G.A., Jonsson, A.K., Stromme M., Barsoukov, Y., Macdonald J.R., (Eds.), In Impedance Spectroscopy (2nd ed), Wiley, New York (2005), pp. 302–326.

50. Schütt. H.J. Solid State Ionics, 505 (1994) 70.

51.Schütt, H.J., Gerdes. E. J. Non-Cryst. Solids, 144 (1992) 1–13.

52. Coelho, R., Physics of Dielectrics. Elsevier Scientific Publishing Company, New York (1979) pp. 97–102

53. Krause, C., Sangoro, J. R., Iacob, C., Kremer. F. J. Phys. Chem. B, 114 (2010) 382.

54. Bandara, T.M.W.J. , Dissanayake, M.A.K.L., Ileperuma, O.A., Varaprathan, K., Vignarooban, K., Mellander. B.-E. J. Solid State Electrochem., 10 (2007) 461.

55. Sorensen, T. S., Diaz-Calleja, R., Riande, E., Guzmán, J., Andrio. A. J. Chem Soc., Faraday Trans., 93 (1997) 2399.

TABLES

Table 1. Chemical composition (% weight) and thickness of films **F1-F5**. Between parentheses we give the experimental ion loading in mmol/g calculated from data of %N experimental. These values are practically the same that the loadings obtained theoretically according to their composition. **%1** represent the amount of 1-(4-vinylbenzyl)-3-butyl imidazolium bistriflamide) VBIM[NTf_2] and **%4** the amount of 1-Butyl-3-methyl imidazolium chloride (BMIM[Cl]), contained into monomeric mixtures based on the styrenic monomer . Finally the corresponding crosslinking agent are indicated by **2** (PEGDMA) and **(3**)TMPTMA, respectively.

SILLP	**Crosslinker** (%)	% **1**	% **4**	**Thickness** (μm)
F1	**2** (20)	80 (1.52)	0	402
F2	**2** (10)	90(1.72)	0	375
F3	**2** (17)	67(1.28)	16(0.91)	405
F4	**3** (10)	45(0.85)	45(2.57)	590
F5	**3** (6)	47(0.91)	47(2.67)	570

Table 2. Values of fit parameters, n, C, R_1, a_1, τ_1, R_2, a_2, τ_2 and R_0 obtained for the samples **F1, F2, F3, F4** and **F5** from the Nyquist plots (i.e. Figure 2a) at 20 and 40 ºC of temperature. The equivalent circuit considered for the fitting is also represented in the inset of the same Figure.

Sample	**T (ºC)**	**n**	**Cx10^6 (F^n)**	**R_1 (Ohms)**	**a_1**	**τ_1x10^3 (s)**	**R_2 (Ohms)**	**a_2**	**τ_2x10^7 (s)**	**R_0 (Ohms)**
F1	20	0,70	0,01	4200	0,81	$3{,}71\times10^{-3}$	-	-	-	-
F1	40	0,73	0,05	3100	0,83	$3{,}00\times10^{-4}$	-	-	-	-
F2	20	0,70	0,01	3900	0,82	$3{,}71\times10^{-3}$	-	-	-	-
F2	40	0,77	0,013	2660	0,84	$2{,}50\times10^{-4}$	-	-	-	-
F3	20	0,60	2,50	160	0,94	4,0	460	0,62	1,0	-
F3	40	0,56	2,50	30	0,90	0,9	102	0,62	0,13	-
F4	20	0,6	100	13	0,8	100	20	0,95	9000	17,9
F4	40	0,62	150	4,00	0,79	60	4,50	0,91	5000	7,50
F5	20	0,5	30	10	1	1,7	22	0,95	180000	11,5
F5	40	0,51	110	2	1	0,9	3,00	0,95	80000	4,60

Table 3. Values of the conductivity obtained from Bode diagram for all the samples and temperatures. σ_1 represent the dc-conductivity at the high frequencies associated to the NTf_2^- anions and σ_2 is the dc-conductivity at moderate frequencies due to the Cl^- ions.

T (ºC)	σ_1 S/cm	σ_1 S/cm	σ_1 S/cm	σ_2 S/cm	σ_1 S/cm	σ_2 S/cm	σ_1 S/cm	σ_2 S/cm
	F1	**F2**	**F3**		**F4**		**F5**	
20	$3.0x10^{-7}$	$3.0x10^{-7}$	$2.8x10^{-5}$	$1.9x10^{-5}$	$1.1x10^{-3}$	$1.1x10^{-5}$	$1.6x10^{-3}$	$1.6x10^{-4}$
30	$1.2x10^{-6}$	$1.3x10^{-6}$	$6.1x10^{-5}$	$2.0x10^{-5}$	$1.6x10^{-3}$	$8.4x10^{-5}$	$2.6x10^{-3}$	$2.3x10^{-4}$
40	$4.0x10^{-6}$	$4.4x10^{-6}$	$1.3x10^{-4}$	$3.9x10^{-5}$	$2.5x10^{-3}$	$1.5x10^{-4}$	$3.9x10^{-3}$	$3.4x10^{-4}$
50	$1.1x10^{-5}$	$1.2x10^{-5}$	$2.3x10^{-4}$	$8.2x10^{-5}$	$3.6x10^{-3}$	$3.2x10^{-4}$	$5.6x10^{-3}$	$3.9x10^{-4}$
60	$2.4\ x10^{-5}$	$2.8\ x10^{-5}$	$3.8x10^{-4}$	$1.1x10^{-4}$	$5.0x10^{-3}$	-	$7.6x10^{-3}$	-
70	$4.8\ x10^{-5}$	$5.7\ x10^{-5}$	$5.8x10^{-4}$	$1.8x10^{-4}$	$6.6x10^{-3}$	-	$9.9x10^{-3}$	-
80	$7.9\ x10^{-5}$	$1.1\ x10^{-4}$	$8.4x10^{-4}$	$2.6x10^{-4}$	$8.5x10^{-3}$	-	$1.3x10^{-2}$	-
90	$1.1\ x10^{-4}$	1.7 x10	$1.1x10^{-3}$	-	$1.1x10^{-2}$	-	$1.5x10^{-2}$	-
100	$1.6\ x10^{-4}$	2.5 x10	$1.4x10^{-3}$	-	$1.3x10^{-2}$	-	$1.8x10^{-2}$	-
110	$2.2\ x10^{-4}$	3.6 x10	$1.6x10^{-3}$	-	$1.5x10^{-2}$	-	$2.1x10^{-2}$	-
120	$3.1\ x10^{-4}$	5.3 x10	$1.9x10^{-3}$	-	$1.8x10^{-2}$	-	$2.4x10^{-2}$	-

Table 4. VFT fit parameters for the conductivity data of the different SILLPs for the whole range of temperature using eq. (2). The values of χ^2 parameters, represent the sum of the squared deviations between experimental values and theoretical values obtained using eq. (3). The values given between parentheses correspond to the fit of the conductivity obtained from moderate frequency (10-100 Hz) may be associated to the free ion (Cl^-), such as seen in the case of the samples F3, F4 and F5. In the sixth column we give the activation energy calculated by means of the fit to Arrhenius behavior of the conductivity values tabulated in table 3 versus 1/T.

SILLP	**ln σ_∞ (S/cm)**	**B (K)**	**T_0 (K)**	**χ^2**	**Eact (kJ/mol)**
F1	-3.65	727	230	0.0394	63.9±2.5
F2	-1.86	998	218	0.0114	69.3±2.5
F3	-2.97	560	219	0.0263	40.3±1.5
		(626)	(212)		46.6±1.5
F4	-0.80	682	182	0.0011	27.3±1.3
		(833)	(186)		44.3±1.6
F5	-1.02	531	196	0.0004	25.8±1.4
		(73)	(264)		34.1±1.8

Table 5. Values of parameter κL, relative bulk dielectric permittivity $\varepsilon_s/\varepsilon_0$, corrected and uncorrected, and τ_{EP} defined by bulk resistance and interfacial capacitance ($\tau_{EP}=R_BC_{EP}$) and relaxation time of the conduction process τ, for all the samples at 20ºC and 50ºC.

Sample	T (ºC)	κL	τ_{EP} (s)	τ (s)	ε_s	ε_{EP}
F1	20	2590	$2.7x10^{-2}$	$8.8x10^{-6}$	71	92000
	50	3900	$1.1x10^{-3}$	$2.7x10^{-7}$	70	137000
F2	20	1270	$8.2x10^{-3}$	$6.7x10^{-6}$	45	28500
	50	1610	$2.3x10^{-4}$	$2.0x10^{-7}$	39	31400
F3	20	5200	$3.7x10^{-3}$	$9.8x10^{-7}$	451	$1.17x10^{6}$
	50	12400	$7.5x10^{-4}$	$5.9x10^{-8}$	315	$1.95x10^{6}$
F4	20	61950	$5.0x10^{-4}$	$1.1x10^{-8}$	203	$6.29x10^{6}$
	50	168200	$4.1x10^{-4}$	$1.7x10^{-9}$	197	$16.6x10^{6}$
F5	20	76800	$5.1x10^{-3}$	$9.0x10^{-6}$	238	$9.14x10^{6}$
	50	197000	$2.3x10^{-4}$	$2.5x10^{-7}$	145	$14.3x10^{6}$

FIGURE CAPTIONS

Figure 1. Synthesis of films **F1**-**F5**.

Figure 2. Nyquist diagrams for the samples: (a) **F1** (black) and **F2** (red), (b) **F3** (green) and (c) **F4** (blue) and **F5** (magenta), respectively at 20ºC and 30ºC. The symbols represent the values experimentally observed and the lines the fit using the electric circuit represented in each figure. Also in each figure we plot the Nyquist diagram in terms of the conductivity at the same temperature.

Figure 3. a) Real part of the conductivity for all the samples (**F1** (●), **F2** (■), **F3** (▲), **F4** (▼) and **F5** (◆)) at 20ºC. b) The phase angle for the samples represented in figure (a). c) Double logarithmic plot of the real part and imaginary part of the conductivity versus frequency for sample F1 and F4 respectively at 30ºC. d) Loss tan δ versus frequency for the same samples plotted in figure (c) at the same temperature. The analysis of electrode polarization show that the peak in loss tan δ is given at the frequency where σ" displays a minimum and the real part of the conductivity a plateau and the phase angle a maximum which tend to value zero. These values have been used to determine the dc-conductivity of the samples. Color code: **F1** (■, black), **F2** (●, red), **F3** (▲, green), **F4** (▼, blue) and **F5** (◆, magenta).

Figure 4. Loss Tangent as a function of frequency (Hz) at 20ºC (left) and 30ºC of temperature (right), for all the samples studied. Symbols code: **F1** (■), **F2** (●), **F3** (▲), **F4** (▼) and **F5** (◆).

Figure 5. Temperature dependenceof conductivity for the different SILLPs. Symbols code: **F1** (■, black), **F2** (●, red), **F3** (▲, green), **F4** (▼, blue) and **F5** (◆, magenta). In samples F3, F4 and F5 we can observe two lines associated to two different processes related with the two conductivities due to different kind of ions: NTf_2^- and Cl^-.

Figure 6. Tan δ values as a function of the perturbation frequency for the different SILLPs at different temperatures, **F1**, **F2** and **F3** from 20ºC to 120ºC, **F4** and **F5** from 20ºC to 50ºC.

Figure 7. Temperature dependence of free ion diffusivity for: a) F1 (■) and F2 (●) samples determined from electrode polarization model according eq (4) (before correction). In open symbols we plot the free ion diffusivity for the same samples after correction. b) Samples F3 (▲), F4 (▼) and F5 (◆) before correction and open symbols after correction.

Figure 8. Temperature dependence of free ion number density *n* for the samples F1 (■), F2 (●), F3 (▲), F4 (▼) and F5 (◆), respectively, calculated from electrode polarization effect using the generalized Trukhan model widely described in references (28-31). Solid lines represent the Arrhenius fits, $n=n_0\ exp(-E_{dis}/k_bT)$.

1.

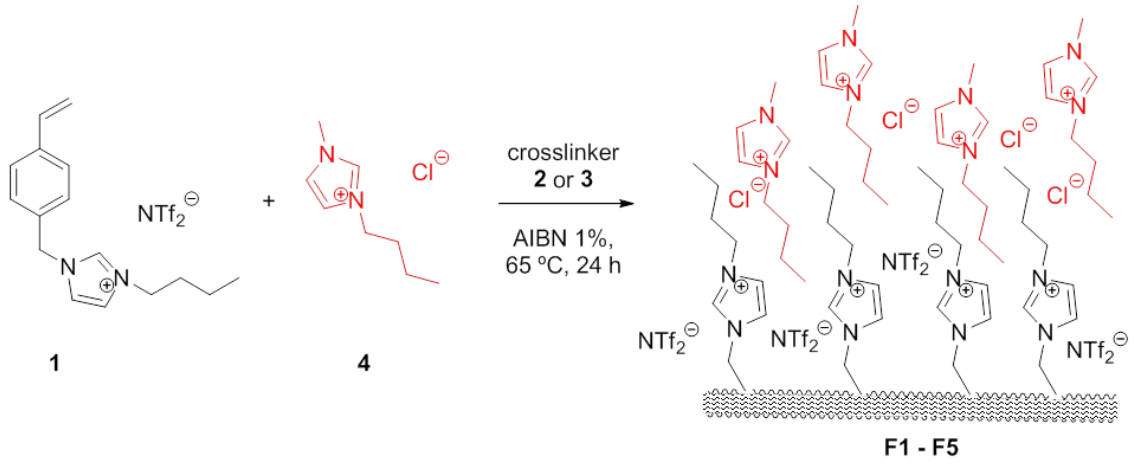

Figure 1.

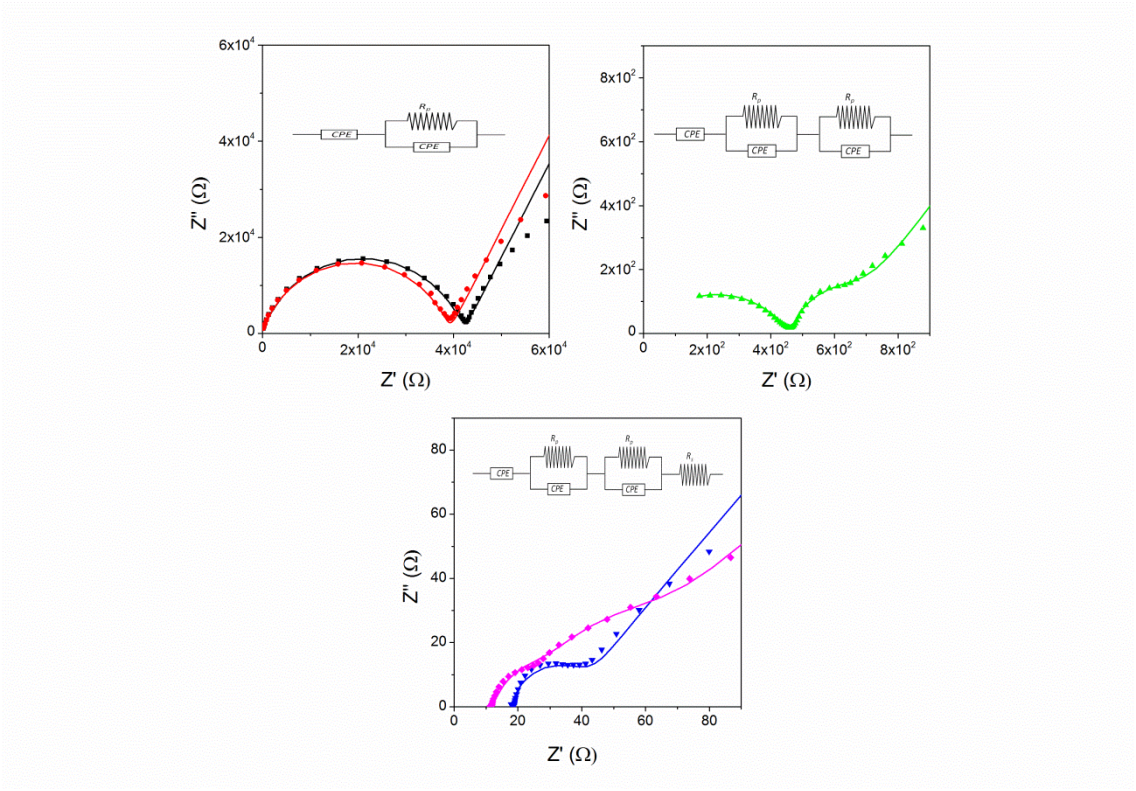

Figure 2.

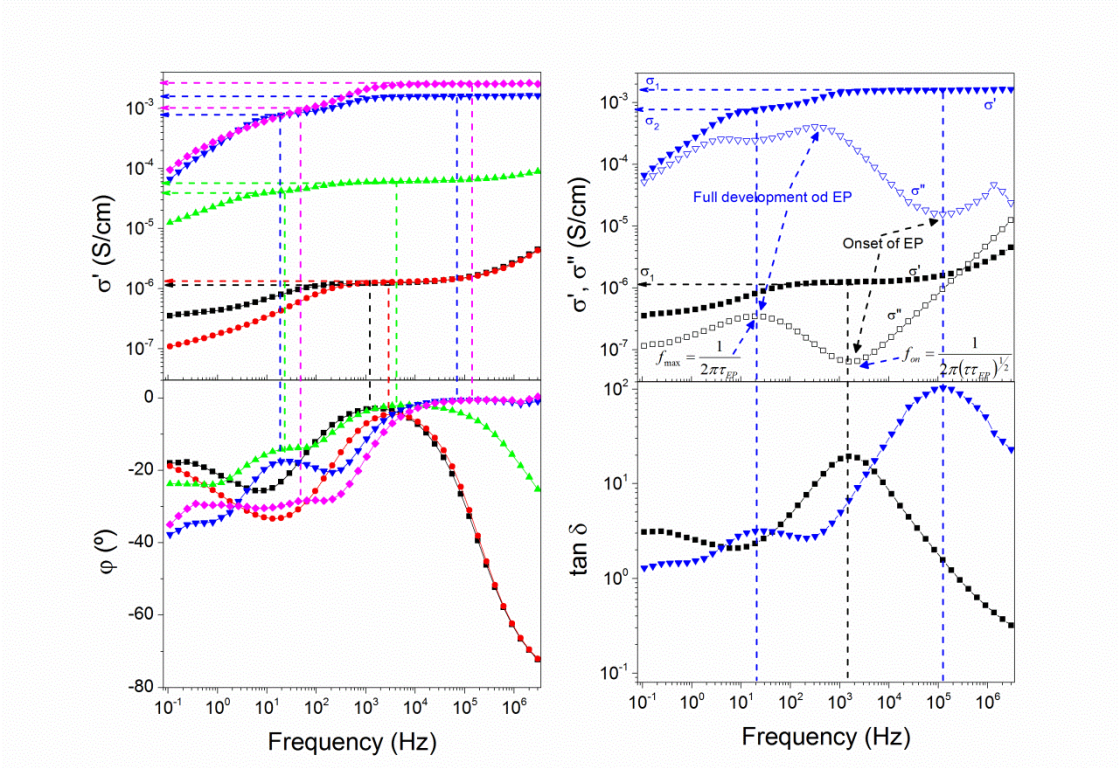

Figure 3.

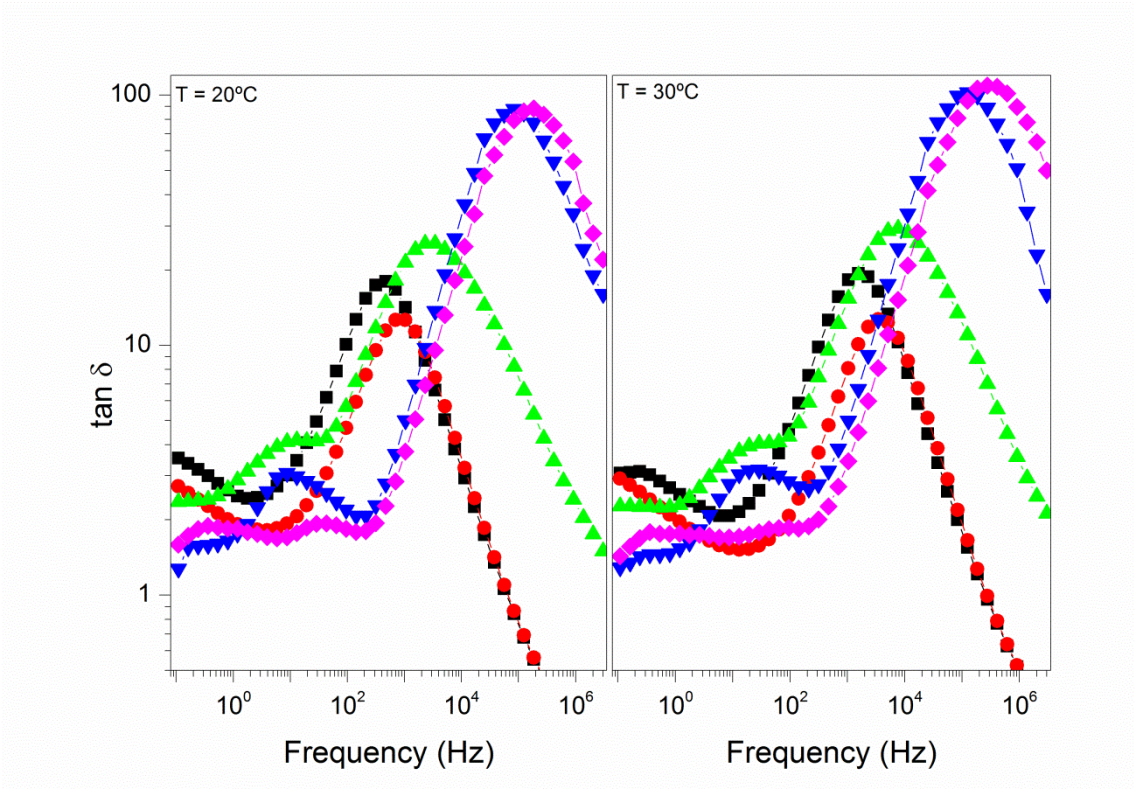

Figure 4.

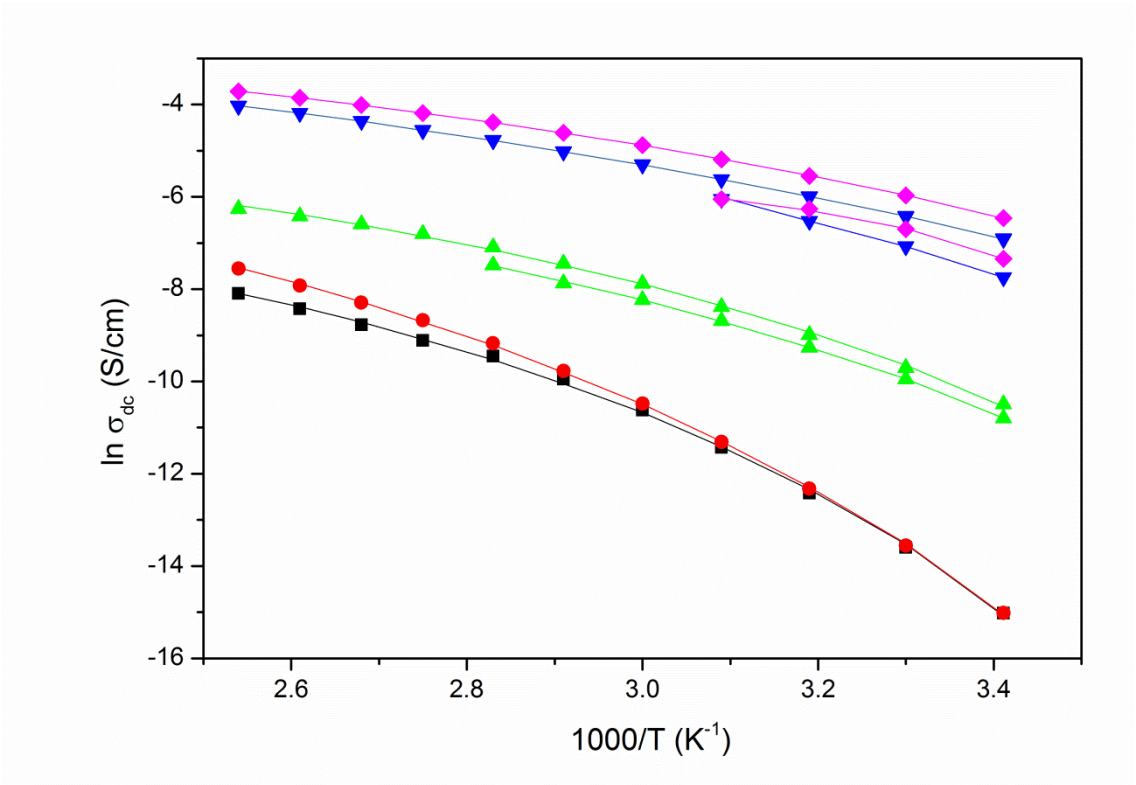

Figure 5.

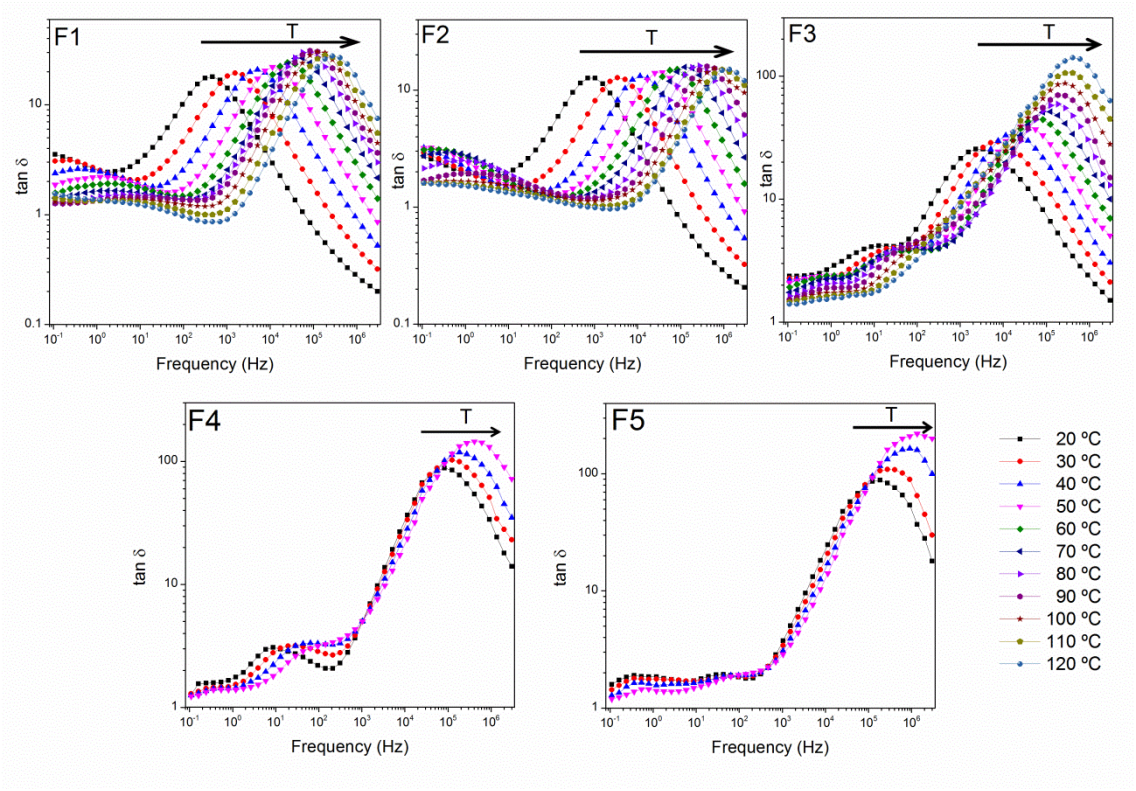
F1
T
tan δ
Frequency (Hz)
F2
T
tan δ
Frequency (Hz)
F3
T
tan δ
Frequency (Hz)
F4
T
tan δ
Frequency (Hz)
F5
T
tan δ
Frequency (Hz)
20 °C
30 °C
40 °C
50 °C
60 °C
70 °C
80 °C
90 °C
100 °C
110 °C
120 °C

Figure 6.

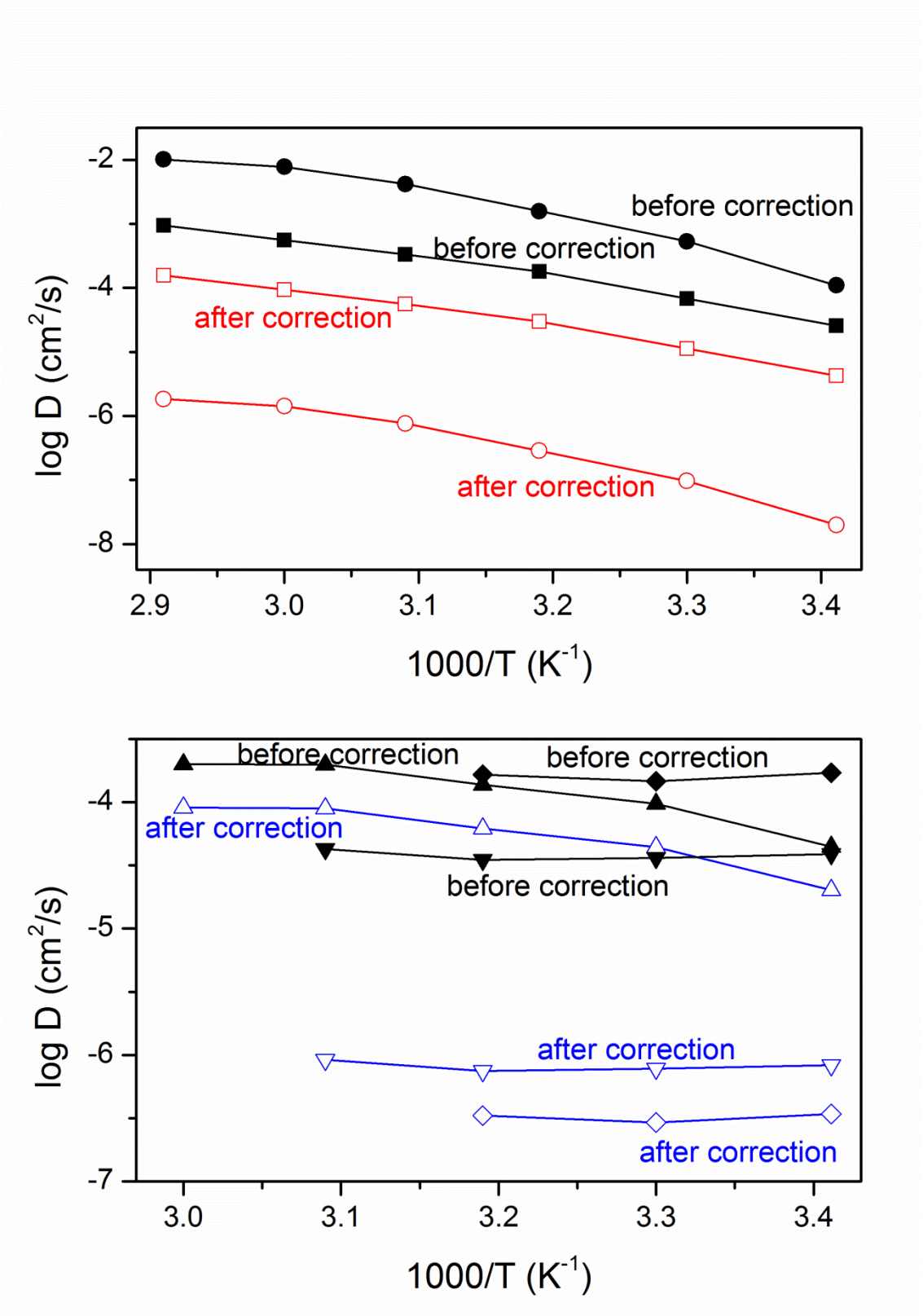
-2
-4
-6
-8
log D (cm²/s)
before correction
before correction
after correction
after correction
2.9
3.0
3.1
3.2
3.3
3.4
1000/T (K⁻¹)
-4
-5
-6
-7
log D (cm²/s)
before correction
before correction
after correction
before correction
after correction
after correction
3.0
3.1
3.2
3.3
3.4
1000/T (K⁻¹)

Figure 7.

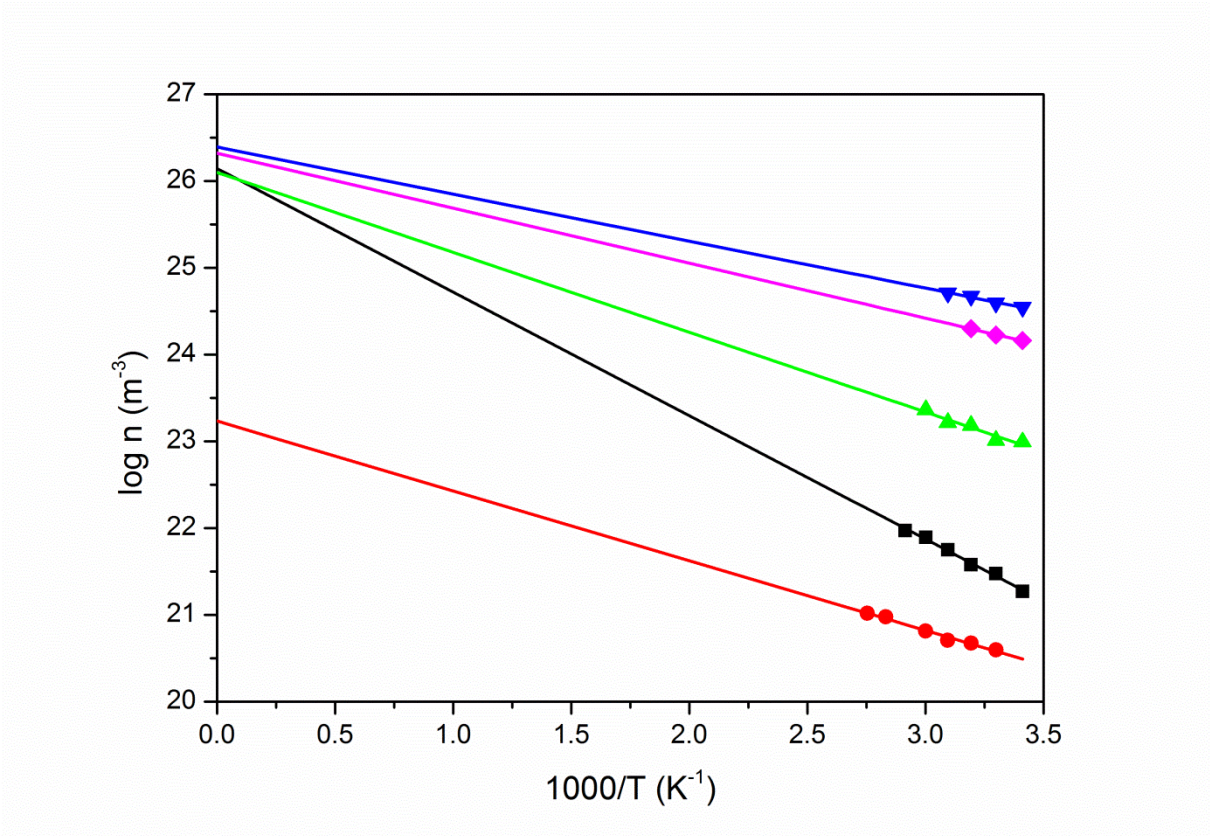

Figure 8.